Bulk Formulation of the Heat and Water Vapor Fluxes at the Air–Sea Interface, Including Nonmolecular Contributions

JAMES A. MUELLER AND FABRICE VERON

College of Marine and Earth Studies, University of Delaware, Newark, Delaware

(Manuscript received 6 January 2009, in final form 17 July 2009)

ABSTRACT

Accurate prediction of the air–sea sensible and latent heat fluxes is vital for nearly all applications of atmosphere and ocean models. Existing theories of heat transfer over rough surfaces provide a starting point, but they seem incomplete given that recent measurements suggest a departure from these theoretically predicted fluxes at higher wind speeds. Although explicit models of the air–sea heat fluxes are desperately needed, the formulation presented in this paper is an attempt to model the air–sea fluxes without dependence on explicit heat flux components. Using smooth flow limit approximations, theoretical profiles, and a physically based surface stress model, the predicted heat fluxes show reasonable agreement with available data. With increasing wind forcing, modestly increasing heat and moisture exchange coefficients (Stanton and Dalton numbers) are found. Even though wave age strongly influences the surface drag, stratification and temperature effects seem to dominate the wave-age influence on the air–sea heat and moisture fluxes.

1. Introduction

The sensible heat and water vapor fluxes at the air–sea interface are important boundary conditions for atmospheric and oceanic models that attempt to capture the physics and evolution of weather and climate. While these fluxes are fairly well known at moderate wind speeds, they remain obscured at the high wind speeds present in storms and hurricanes. Recent measurements at high wind speeds from the Coupled Boundary Layer and Air–Sea Transfer (CBLAST; Drennan et al. 2007; Zhang et al. 2008) experiment only seem to complicate our already limited understanding. These studies find a lower ratio of the enthalpy and momentum transfer coefficients than both the theoretical prediction by Emanuel (1995) for hurricane development and sustainability and the current implemented value in hurricane models. Consequently, there is no empirically verified theory that explains how hurricanes overcome the drag of the ocean surface to become the familiar massive, swirling disasters. Although the CBLAST results challenge existing theories, the high level of uncertainty in the data prohibits any strong conclusion, such as the refutation of Emanuel (1995).

Under hurricane conditions, frequent wave-breaking, along with airflow and surface separation, produces sea spray in the air and foam in the water. Potentially, the underlying physics could be dramatically different than that at lower wind speeds where most of the empirical data exist. Most studies that include an additional distinct route for transfer via sea spray (e.g., Andreas and Emanuel 2001; Andreas et al. 2008; Perrie et al. 2005) find an effective ratio of the total (interfacial and spray-mediated) enthalpy and momentum transfer coefficients above 0.75 that is consistent with Emanuel (1995). Although derived empirically from data at moderate wind speeds, these estimates of spray effects at higher wind speeds depend on three main components: an extrapolated sea spray generation function to higher wind speeds, a modeled interfacial component at high wind speeds, and accurate estimates of the spray-mediated fluxes and microphysics at moderate wind speeds.

While the microphysical model is physically based and robust, Andreas et al. (2008) estimate the spray-mediated fluxes at moderate wind speeds by tuning their microphysical model to account for the residual fluxes, which are found by subtracting the modeled interfacial components from the empirical measured fluxes. If the model of the interfacial fluxes is wrong at moderate wind speeds, the spray-mediated fluxes will be incorrect before any extrapolation to higher wind speeds. Therefore,

Corresponding author address: Fabrice Veron, 112C Robinson Hall, University of Delaware, Newark, DE 19716.
E-mail: fveron@udel.edu

DOI: 10.1175/2009JAS3061.1

an investigation of these relevant physical mechanisms seems imperative. Toward that aim, this paper is an attempt to model the interfacial component of the heat and water vapor fluxes from low to high wind speeds.

Early models of the air–sea boundary layer relied heavily on the vast studies concerning flow over rigid surfaces. In recent years, the deviation of the air–sea surface stress from the rigid surface stress has received considerable attention. The deviation of the air–sea heat and mass surface fluxes from those over rigid surfaces, however, is only beginning to garner serious attention. Nevertheless, the wealth of knowledge for the rigid, rough surface case (e.g., Owen and Thomson 1963; Brutsaert 1982; Zilitinkevich et al. 2001) provides a starting point for the air–sea heat and water vapor fluxes. Accordingly, the increase in the rate of heat and water vapor transfer due to an increasingly rough surface is less than that of momentum. Whereas the surface stress is augmented by the roughness, resulting in form drag, the rate of scalar transport at a rigid surface is still controlled by molecular forces. In other words, heat and water vapor transfer at the surface are controlled by conduction and molecular diffusion, regardless of surface irregularity or roughness of the turbulent flow. This does not mean that the transfer rate is always equivalent to the smooth flow case, however.

The roughness of the flow can modulate the temperature and water vapor profiles, altering the gradients and corresponding fluxes at the surface. The modulation of the temperature and water vapor profiles by the roughness of the flow is a part of the model presented below. Furthermore, the air–sea interface, unlike the rigid boundary layer case, is a boundary between two fluids. The scalar fluxes in and out of a deforming, evolving surface could deviate substantially from our current understanding. Although there seems to be experimental evidence for such a significant deviation (Veron et al. 2008), no well-developed theory exists to explain it. The model presented here does not attempt to address this deviation directly, but it does attempt to provide a framework for modeling the heat and water vapor fluxes through the air–sea interface.

To extend the interfacial scalar flux to the frequent wave breaking regime at high wind speeds, our model combines a physically based model of the stress at the air–sea interface with previous models of the scalar molecular layers from surface renewal theory (e.g., Clayson et al. 1996; Fairall et al. 2000; Soloviev and Schluessel 1994). We calculate the molecular contributions to the scalar fluxes following the formulation of the viscous stress for the momentum flux (see Mueller and Veron 2009): we first calculate the equivalent flux for smooth flow. Then we modify this flux, accounting for sheltering from airflow separation.

The nonmolecular components of the scalar fluxes, however, cannot be treated explicitly like their momentum counterparts. In the absence of an explicit treatment, the nonmolecular components of the scalar fluxes are estimated to be the difference between the total flux and the molecular flux. The focus on the distinct scalar flux components distinguishes this model from previous ones. Unlike most models, the roughness length is only prescribed to find the equivalent molecular fluxes in smooth flow. The nonmolecular fluxes are explicitly modeled for momentum and approximated for scalars.

2. Model description

The bulk parameterization of air–sea fluxes relates the momentum, heat, and water vapor fluxes at the interface to measurable variables:

$$\begin{aligned} \tau &= -\rho\overline{u'w'} = \rho C_D(U_{10} - U_0)|U_{10} - U_0|, \\ H &= -\rho c_p\overline{\theta'w'} = \rho c_p C_H(\theta_{10} - \theta_0)|U_{10} - U_0|, \quad \text{and} \\ M &= -\rho\overline{q'w'} = \rho C_E(q_{10} - q_0)|U_{10} - U_0|, \end{aligned} \tag{1}$$

where ρ and c_p are the density and isobaric specific heat of air, respectively. The primes indicate turbulent quantities, and the overbars represent ensemble averages. The respective flux scales for velocity, potential temperature, and specific humidity are u_*, θ_*, and q_* and relate to the turbulent fluxes as $u_*|u_*| = -\overline{u'w'}$, $\theta_*|u_*| = -\overline{\theta'w'}$, and $q_*|u_*| = -\overline{q'w'}$. The transfer coefficients for momentum, heat, and moisture at 10-m height are C_D, C_H, and C_E and are usually referred to as the drag coefficient, Stanton number, and Dalton number. The subscript 0 indicates the value at the interface; the subscript 10 is the 10-m height value. Note the sign convention in Eq. (1), in which positive fluxes are into the ocean and negative fluxes are out of the ocean and into the atmosphere. Finally, the latent heat flux is $E = L_v M$, where L_v is the latent heat of vaporization.

Outside the viscous and wave boundary layers and under the assumption that the fluxes are constant up to a given height, the respective flux budget equations can be integrated to obtain similarity profiles for mean wind speed, potential temperature, and specific humidity:

$$\begin{aligned} U(z) - U_0 &= \frac{u_*}{\kappa}\left[\ln\left(\frac{z+\delta_m}{z_m}\right) - \Psi_m\left(\frac{z}{L}\right)\right], \\ \theta(z) - \theta_0 &= \frac{\theta_*}{\kappa}\left[\ln\left(\frac{z+\delta_\theta}{z_\theta}\right) - \Psi_\theta\left(\frac{z}{L}\right)\right], \quad \text{and} \\ q(z) - q_0 &= \frac{q_*}{\kappa}\left[\ln\left(\frac{z+\delta_q}{z_q}\right) - \Psi_q\left(\frac{z}{L}\right)\right], \end{aligned} \tag{2}$$

where $\kappa \approx 0.4$ is the Von Kármán constant and z_m, z_θ, and z_q are the roughness lengths of momentum, potential temperature, and specific humidity, respectively. The variable $\delta_i = \alpha_i z_i$ ($i \in \{m, \theta, q\}$), usually with $\alpha_i = 1$, is introduced such that the profile is not singular at the interface ($z = 0$). The stability functions, Ψ_m, Ψ_θ, and Ψ_q, are corrections to the profiles that account for the stratification in the boundary layer and are functions of the height z and the Obukhov length (i.e., the height at which shear production of turbulent kinetic energy balances buoyant production):

$$L = \frac{u_*^3 \theta}{g\kappa u_* [\theta_* (1 + 0.6078 q_0) + 0.6078 q_* \theta]}, \tag{3}$$

where $g \approx 9.81$ is the constant of gravitational acceleration. The form of the stability functions are taken from the Tropical Ocean Global Atmosphere Coupled Ocean–Atmosphere Response Experiment (TOGA COARE) 3.0 algorithm (Fairall et al. 2003; Grachev et al. 2000), which is based on Businger et al. (1971) and Beljaars and Holtslag (1991).

a. Momentum flux

Under most conditions, the turbulent momentum flux dominates the air–sea fluxes of heat and mass; in other words, the turbulent structure of the velocity field and corresponding transport control the scalar fluxes for a given bulk scalar gradient. Consequently, before considering the heat and water vapor fluxes, the momentum flux must first be modeled. The total surface stress, τ, can be divided into three main components (viscous, wave-induced, and separation):

$$\tau|_{z=0} = \tau_\nu + \tau_w + \tau_s, \tag{4}$$

where τ_ν, τ_w, and τ_s are the viscous, wave-induced, and separation stresses, respectively, and are modeled according to Mueller and Veron (2009) in which the two-dimensional, empirical surface wave spectrum follows Elfouhaily et al. (1997) and the separation stress is parameterized similarly to Kudryavtsev and Makin (2007). Although we choose the surface stress model from Mueller and Veron (2009), any other stress model that determines surface values for both τ and τ_ν can be used. Under the assumption that the flux is constant within the boundary layer, the total stress at any given height is equivalent to the stress at the surface:

$$\tau(z) = \tau(z)|_{z=0} = \tau_\nu(z) + \tau_w(z) + \tau_s(z) + \tau_t(z), \tag{5}$$

where τ_t is the turbulent stress. With τ, U_{10}, and U_0, the roughness length is implicitly defined from the velocity profile (Mueller and Veron 2009):

$$z_m = \exp[\ln(10 + \delta_m) - \Psi_m - u_*^{-1}\kappa(U_{10} - U_0)], \tag{6}$$

with

$$\delta_m = z_m \exp(A\kappa u_{*_\nu} u_*^{-1} \sqrt{|\tau_\nu \tau^{-1}|}), \tag{7}$$

where $A = 10$ is the height of the viscous sublayer in wall coordinates, $z^+ = z|u_*|/\nu$, with ν being the kinematic viscosity of air; $\tau_\nu = \rho u_{*_\nu} |u_{*_\nu}|$ represents the viscous component of the surface stress. Again, any other surface stress model or drag coefficient relationship could easily be substituted.

b. Heat and moisture fluxes

Following the momentum flux, the surface heat and moisture fluxes can be split into multiple components (molecular, wave-induced, separation):

$$\begin{aligned} H|_{z=0} &= H_{\text{mol}} + H_w + H_s, \quad \text{and} \\ M|_{z=0} &= M_{\text{mol}} + M_w + M_s, \end{aligned} \tag{8}$$

where the subscripts mol, w, and s denote the molecular, wave-induced, and separation components of the heat and moisture fluxes, respectively. Although both numerical simulations and field experiments (Sullivan and McWilliams 2002; Veron et al. 2008) suggest evidence for a wave-coherent heat flux H_w, no well-developed theory for that phenomenon exists. In fact, some authors postulate that waves cannot play a direct role in the transfer of heat and moisture because there is no equivalent to form drag in the heat and mass transfer equations (Makin et al. 1995). Nevertheless, the transfer of heat and mass is indisputably dependent on the turbulent flow, which is known to be modulated by the presence of waves (e.g., Belcher and Hunt 1998; Sullivan and McWilliams 2002). Because there is little to no theoretical foundation to model the wave-coherent heat and moisture fluxes, we must take a different approach from the momentum case, in which the partitioned flux components are directly modeled (e.g., Mueller and Veron 2009). The rest of this section describes this approach.

From Eq. (1), the heat and moisture fluxes are proportional to the covariances of the vertical velocity and the temperature and specific humidity, respectively. While this is valid at sufficient heights where measurements are routinely made, molecular forces dominate near the surface. The heat and moisture fluxes valid throughout the boundary layer are

$$\begin{aligned} H &= \rho c_p \left(-\overline{\theta' w'} + K \frac{\partial \theta}{\partial z} \right) \quad \text{and} \\ M &= \rho \left(-\overline{q' w'} + \epsilon \frac{\partial q}{\partial z} \right), \end{aligned} \tag{9}$$

where K and ϵ are the molecular diffusivities of heat and water vapor in air, respectively. In other words, the gradients of potential temperature and specific humidity determine the molecular fluxes. Therefore, the molecular sublayer profiles need to be modeled for the fluxes to be correct down to the surface.

Analogous to the momentum case, the linear molecular sublayer with a smooth transition to the log layer for both temperature and specific humidity can be approximated by the van Driest damping function (van Driest 1956):

$$\frac{\theta(z^+) - \theta_0}{\theta_*} = B\left[1 - \exp\left(\frac{-\mathrm{Pr}z^+}{B}\right)\right]$$
$$\frac{q(z^+) - q_0}{q_*} = C\left[1 - \exp\left(\frac{-\mathrm{Sc}z^+}{C}\right)\right], \tag{10}$$

where $B = A\mathrm{Pr}^{1/2}$ and $C = A\mathrm{Sc}^{1/2}$ are the heights of the molecular layers in wall coordinates (Liu et al. 1979), and $\mathrm{Pr} = \nu/K$ and $\mathrm{Sc} = \nu/\epsilon$ are respectively the Prandtl (≈0.72 at 20°C) and Schmidt (≈0.63 at 20°C) numbers. The complete profiles can then be taken as the summation of the linear sublayer approximations and the logarithmic layers that are exponentially damped in the near-wall region, as follows:

$$\theta(z) - \theta_0 = B\theta_*\left[1 - \exp\left(\frac{-\mathrm{Pr}z^+}{B}\right)\right]\left|\frac{u_{*_\nu}}{u_*}\right| + \frac{\theta_*}{\kappa}\left[\ln\left(\frac{z+\delta_\theta}{\delta_\theta}\right) - \Psi_\theta\right] \times \left[1 - \exp\left(\frac{-\mathrm{Pr}z^+}{B}\right)\right], \quad \text{and}$$

$$q(z) - q_0 = Cq_*\left[1 - \exp\left(\frac{-\mathrm{Sc}z^+}{C}\right)\right]\left|\frac{u_{*_\nu}}{u_*}\right| + \frac{q_*}{\kappa}\left[\ln\left(\frac{z+\delta_q}{\delta_q}\right) - \Psi_q\right] \times \left[1 - \exp\left(\frac{-\mathrm{Sc}z^+}{C}\right)\right]. \tag{11}$$

The profile form given in Eq. (11) offers a continuous (and second-order differentiable) formulation that smoothly connects the molecular (linear) and log layers. The modification of the van Driest component accounts for the roughness of the flow and converges to the standard definition given in Eq. (10) for the smooth flow limit, thereby converging to the surface limit (i.e., $z^+ \to 0$), which yields $(\theta - \theta_0)/\theta_* = \mathrm{Pr}z^+|u_{*_\nu}/u_*|$ and $(q - q_0)/q_* = \mathrm{Sc}z^+|u_{*_\nu}/u_*|$. In the smooth flow limit where the surface stress is entirely due to viscosity, the surface limits further reduce to $(\theta - \theta_0)/\theta_* = \mathrm{Pr}z^+$ and $(q - q_0)/q_* = \mathrm{Sc}z^+$. Accordingly, the kinematic molecular fluxes at the surface are $Kd\theta/dz|_{z=0} = \theta_*|u_{*_\nu}|$ and $\epsilon dq/dz|_{z=0} = q_*|u_{*_\nu}|$.

Outside the molecular sublayers, the profiles converge to the nonsingular, standard log layers from Eq. (2), with

$$\alpha_\theta = \exp\left(\kappa B\sqrt{\left|\frac{\tau_\nu}{\tau}\right|}\right) \quad \text{and}$$
$$\alpha_q = \exp\left(\kappa C\sqrt{\left|\frac{\tau_\nu}{\tau}\right|}\right). \tag{12}$$

The coefficients α_θ and α_q merely shift the profiles near the surface in order to match the linear sublayer approximations to the log layers. At the upper limit $z^+ \to \infty$, the profiles converge to the standard log layers:

$$\theta(z) - \theta_0 = \frac{\theta_*}{\kappa}\left[\ln\left(\frac{z}{z_\theta}\right) - \Psi_\theta\right] \quad \text{and}$$
$$q(z) - q_0 = \frac{q_*}{\kappa}\left[\ln\left(\frac{z}{z_q}\right) - \Psi_q\right]. \tag{13}$$

With the profile forms for velocity, potential temperature, and specific humidity as well as the surface and 10-m values, the surface fluxes can either be modeled or found from prescriptions of the roughness length. As noted earlier, we model the surface stress according to Mueller and Veron (2009) but are unable to model the heat and moisture fluxes directly. Instead, we take the following approach. We solve for the fluxes in the rigid, smooth boundary layer limit (τ^0, H^0, and M^0) by prescribing the smooth flow limit roughness lengths:

$$z_m = \frac{\nu}{|u_*|}z_m^+ = \frac{\nu}{|u_*|}\exp(-5.5\kappa) \approx 0.11\frac{\nu}{|u_*|},$$
$$z_\theta = \frac{\nu}{|u_*|}z_\theta^+ = \frac{\nu}{|u_*|}\exp(-5.5\mathrm{Pr}\kappa) \approx 0.21\frac{\nu}{|u_*|}, \quad \text{and}$$
$$z_q = \frac{\nu}{|u_*|}z_q^+ = \frac{\nu}{|u_*|}\exp(-5.5\mathrm{Sc}\kappa) \approx 0.25\frac{\nu}{|u_*|}, \tag{14}$$

where the velocity intercept in wall coordinates is taken to be 5.5 as suggested by Hinze (1975). The temperature and humidity intercepts in wall coordinates are only shifted by the Prandtl and Schmidt numbers, respectively, and fall within the conventional range of values.

After solving for θ_* and q_* in this smooth flow case, we then proceed to the model the air–sea surface stress, as $\tau \neq \tau^0 \neq \tau_\nu$ because of the roughness of the flow. With the fraction of sheltered area due to airflow separation f

the viscous stress is assumed to be $\tau_\nu = (1 - f)\tau^0$. With θ_* and q_* fixed to their smooth flow values while modeling u_* and u_{*_ν}, we find the molecular components of the scalar fluxes ($H_{\text{mol}} = \theta_*|u_{*_\nu}|$ and $M_{\text{mol}} = q_*|u_{*_\nu}|$) as well as the total fluxes ($H = \theta_*|u_*|$ and $M = q_*|u_*|$). The roughness lengths in the rough, wavy flow are implicitly defined, and the nonmolecular components of the heat and mass fluxes are taken to be $H_w + H_s = H - H_{\text{mol}}$ and $M_w + M_s = M - M_{\text{mol}}$, respectively. Because the profiles and surface stress change with flow roughness, the resulting scalar roughness lengths are not necessarily equal to those at the smooth flow limit.

As presented in the next section, the smooth flow values of θ_* and q_* seem to be fairly good approximations; in other words, θ_* and q_* do not seem to be heavily dependent on the roughness of the flow. The heat and mass fluxes do depend on the flow roughness, but their dependence is assumed to be dominated by the surface stress. Therefore, as long as the surface stress is modeled or measured correctly, the heat and moisture fluxes seem to be relatively more straightforward to predict.

3. Empirical validation

The results of the model described above are compared to experimental data from TOGA COARE (Fairall et al. 1996a, 1997), the San Clemente Ocean Probing Experiment (SCOPE; Fairall et al. 1996b), the Humidity Exchange over the Sea (HEXOS; DeCosmo et al. 1996) experiment, and the CBLAST (Zhang et al. 2008; Drennan et al. 2007) experiment. For the following model runs, the 10-m temperature and relative humidity are 20°C and 80%, respectively. Although these values are not representative of any particular experiment, they are representative of the data ranges to which the model is compared. For example, typical air temperatures from HEXOS are colder by the same amount that the air temperatures from CBLAST are warmer. In neutral stratification, a ±10°C change in temperature leads to a change in scalar roughness lengths of ±8.5% at $U_{10} = 10$ m s^{-1} and ±6% at $U_{10} = 50$ m s^{-1}, as well as a change in Stanton and Dalton numbers of ±4.5% at $U_{10} = 5$ m s^{-1} and less than ±1% at $U_{10} = 50$ m s^{-1}. Also, the relative humidity at the surface is set constant at 98%, as found over seawater. Unless otherwise noted, the fetch used in our stress model is 100 km.

With the sea-state and boundary conditions fixed, we consider a range of wind speeds and surface temperatures, with the air–sea temperature difference expressed as $\Delta\theta = \theta_{10} - \theta_0$. The drag coefficient is plotted in Fig. 1a. Mueller and Veron (2009) discuss this modeled drag coefficient in more detail for the neutral stratification case. The modeled drag coefficient follows the regression line from Taylor and Yelland (2000) until roughly 20 m s^{-1}, when it begins to saturate. Although our model does not predict a completely flat or decreasing drag coefficient at high wind speeds as suggested by Donelan et al. (2004) or Powell et al. (2003), it shows a strong departure from the extrapolated coefficients. At high wind speeds, the effect of mild stratification naturally becomes insignificant, as seen by the convergence of all cases considered.

Figures 1b and 1c show the Stanton and Dalton numbers, respectively. At moderate wind speeds, both fall within the range of the HEXOS data. At high wind speeds, both completely saturate toward the higher end of the CBLAST[1] range. Although the data from HEXOS and CBLAST suggest both coefficients are constant at wind speeds above 10 m s^{-1}, this remains an unresolved issue (see, e.g., Sahlee et al. 2008). Certainly, if the transfer coefficients increase at all, one would expect an increase to occur in the 10–20 m s^{-1} wind speed range, especially with augmented heat (and water vapor) fluxes due to surface waves as suggested by Veron et al. (2008).

Finally, the ratio of the Dalton number and drag coefficient is shown in Fig. 1d. For reference, the HEXOS and CBLAST data, as reported in Zhang et al. (2008), are also plotted. Though still below the theoretical threshold value 0.75, under which Emanuel (1995) suggested hurricanes cannot be sustained, our model produces ratios close to the experimental results. Recently, Smith et al. (2008), for example, raised questions about the validity of the Emanuel (1995) potential intensity model for hurricanes. Unfortunately, the data are not precise enough to settle this debate. If we were to assume that the 0.75 threshold holds, we would find that any overestimation in the Dalton number is matched by a similar overestimation in the drag coefficient. Under this assumption, the controlling factor of the air–sea fluxes seems to be surface stress.

Previous studies have found a distinct relationship between the drag coefficient and the Dalton number. Intuitively, the friction velocity, found in the water vapor flux term far from the surface, is proportional to the drag coefficient to the one-half power. Solving for the scalar exchange coefficients in Eq. (1) and substituting the drag coefficient and flux scales, one finds

[1] We use one standard deviation to illustrate the range of the CBLAST data instead of one standard error as presented in Zhang et al. (2008) and Drennan et al. (2007). Not only is this consistent with our presentation of the HEXOS data, but we also believe its use to be more appropriate here. Standard error, though a useful statistical measure, does not estimate the data scatter or variability; instead, it estimates the deviation of the mean estimate from its actual real world value.

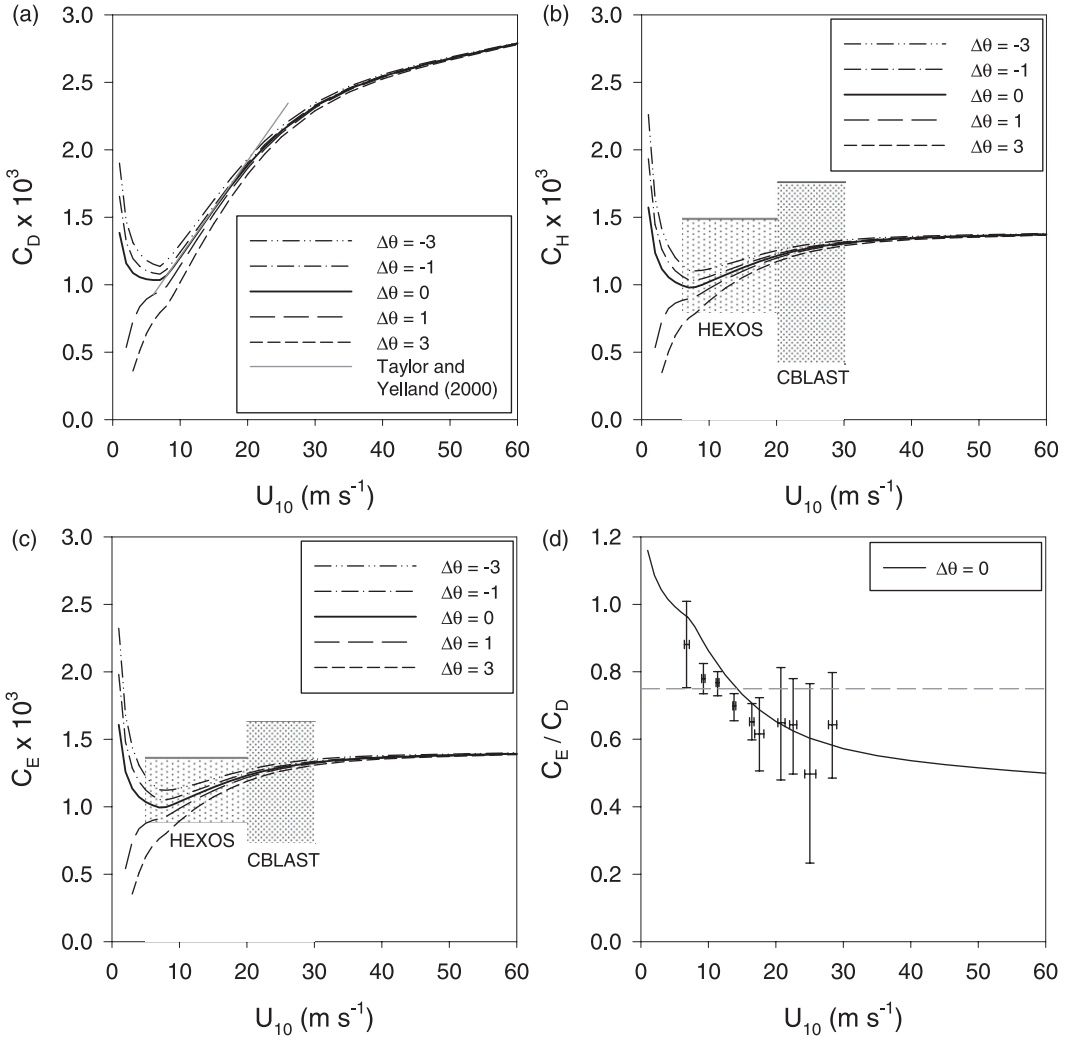

FIG. 1. (a) Drag coefficient, (b) Stanton number, and (c) Dalton number as a function of wind speed for $\Delta\theta = -3$°C (dashed–double dotted), −1°C (dashed–dotted), 0°C (solid), 1°C (long dashed), and 3°C (short dashed) (d) The ratio of the Dalton number and drag coefficient for $\Delta\theta = 0$°C (solid). For reference, the drag coefficient of Taylor and Yelland (2000) as well as the HEXOS and CBLAST data with confidence intervals are shown. The gray dashed line is the threshold value 0.75 from Emanuel (1995).

$$C_H = \frac{\theta_*}{\theta_{10} - \theta_0} C_D^{1/2} \quad \text{and}$$

$$C_E = \frac{q_*}{q_{10} - q_0} C_D^{1/2}. \tag{15}$$

Indeed, Large and Pond (1982) and DeCosmo et al. (1996) found such a relationship in their data. Figure 2a shows the modeled Stanton number divided by the drag coefficient to the one-half power as a function of wind speed and, for reference, the empirical relationship from Large and Pond (1982). At low wind speeds, the model finds a similar relationship for the unstable stratification cases, which occur when the sea surface is warmer than the air. For most of the wind speeds, however, our model predicts a smaller value than Large and Pond (1982). Smaller values mean the normalized wind stress relationship contributes more to the Stanton number than the normalized air–sea temperature difference. Both the model and the empirical relationship from Large and Pond (1982) indicate the importance of the momentum flux to the normalized heat flux.

Figure 2b shows the modeled Dalton number divided by the drag coefficient to the one-half power as a function of wind speed and, for reference, the empirical relationships from Large and Pond (1982) and HEXOS. The HEXOS relationship depends on the drag coefficient and consequently has a wind speed dependence. For its calculation,

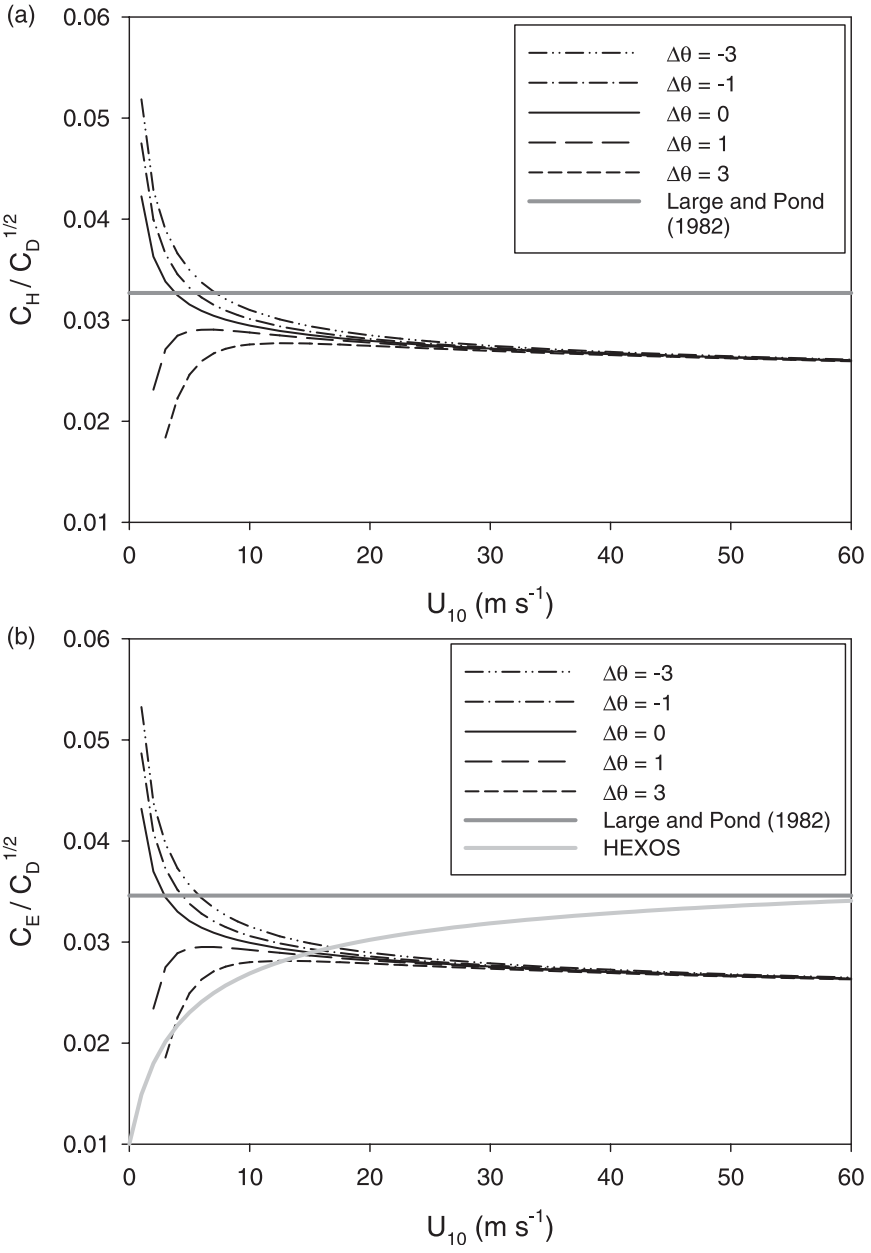

FIG. 2. (a) Stanton number and (b) Dalton number divided by the square root of the drag coefficient as a function of wind speed for $\Delta\theta = -3$°C (dashed–double dotted), -1°C (dashed–dotted), 0°C (solid), 1°C (long dashed), and $\Delta\theta = 3$°C (short dash) as well as relationships from HEXOS (thick light gray) and Large and Pond (1982; thick dark gray).

the HEXOS drag coefficient was used and extrapolated to high wind speeds. At high wind speeds, this extrapolated drag coefficient is much greater than the drag coefficient predicted by our model. Nevertheless, the model values fall between those of the two empirical relationships. At moderate and high wind speeds, the model values are smaller than both of them. Again, smaller values mean the drag coefficient has more relative importance to the Dalton number. Because our modeled drag coefficient saturates at moderate to high wind speeds, the Stanton and Dalton numbers also saturate, as seen in Fig. 1. The Stanton and Dalton numbers may also become slightly more independent of the drag coefficient at higher wind speeds, but that conclusion needs more evidence.

To further illustrate the relationship between surface stress and scalar fluxes, we next consider the ratio of the

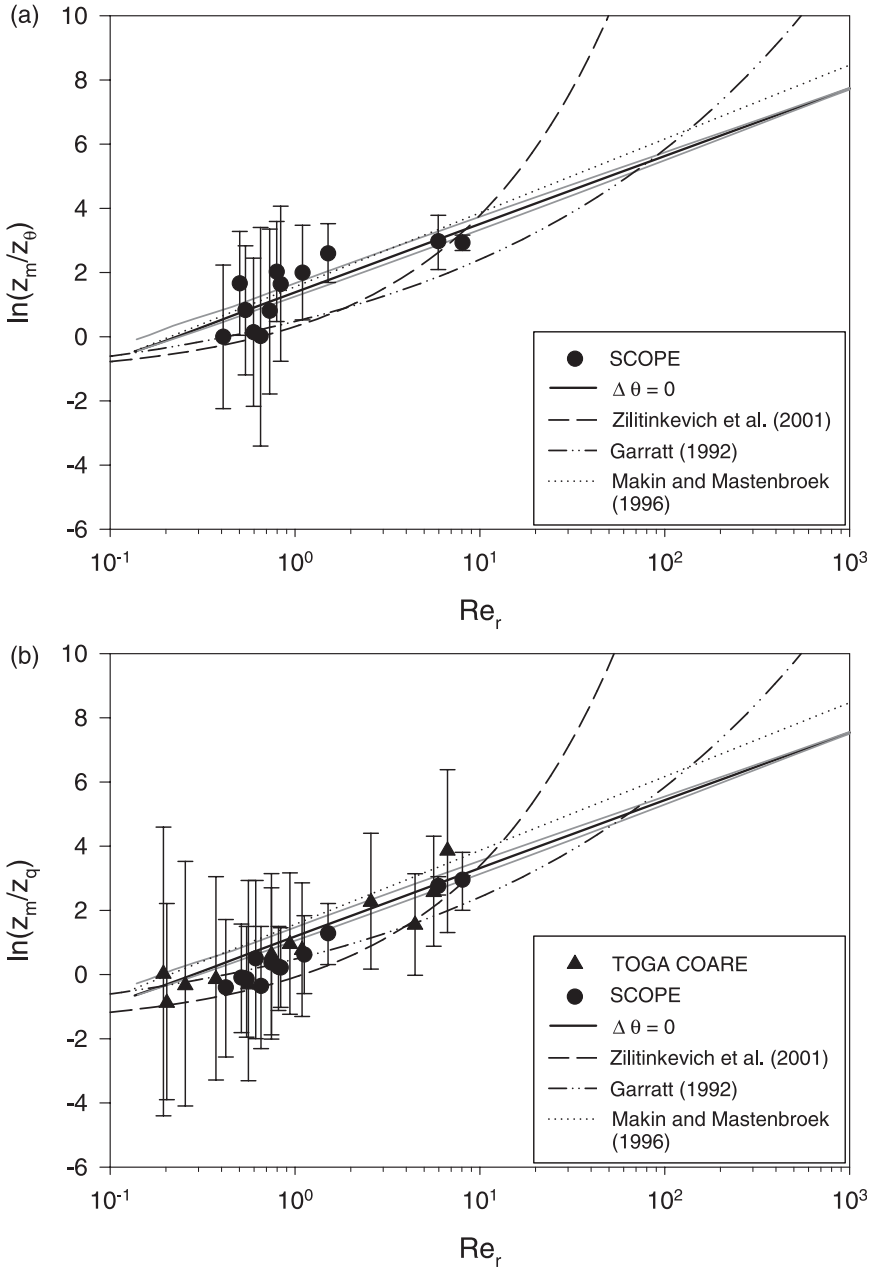

FIG. 3. Ratio of the roughness lengths for (a) momentum and temperature and (b) momentum and water vapor as a function of the roughness Reynolds number for $\Delta\theta = 0$°C (black line), 3°C (upper gray line), and −3°C (lower gray line). Data from SCOPE (circles) and TOGA COARE (triangles) are also shown along with model results from Zilitinkevich et al. (2001; dashed), Garratt (1992; dashed–dotted) and Makin and Mastenbroek (1996; dotted).

momentum roughness length to the scalar roughness lengths. In many models, the scalar fluxes are modeled from the momentum roughness length and the roughness Reynolds number, $\mathrm{Re}_r = z_m|u_*|/\nu$. Figures 3a and 3b show the ratio of the momentum roughness length to the temperature and water vapor roughness lengths, respectively, as a function of roughness Reynolds number. For reference, data from TOGA COARE (Fairall et al. 1996a, 1997) and SCOPE (Fairall et al. 1996b) are included along with model results from Zilitinkevich et al. (2001), Garratt (1992), and Makin and Mastenbroek (1996).

In Fig. 3a, all of the models converge to the smooth flow limit (≈ -0.8), defined at $\mathrm{Re}_r = 0.1$. This is not the

case in Fig. 3b, in which only our model and that from Zilitinkevich et al. (2001) approach the smooth flow limit (≈ -1.2); the models of Garratt (1992) and Makin and Mastenbroek (1996) assume that the temperature and water vapor roughness lengths are the same (i.e., Pr = Sc). At the other end, only the models of Zilitinkevich et al. (2001) and Makin and Mastenbroek (1996) fit the data of the roughest flows as well as our model for both temperature and water vapor roughness lengths. For $\mathrm{Re}_r > 100$, our model departs from all of the models except that of Makin and Mastenbroek (1996). From the Powell et al. (2003) data, typical values for Re_r in hurricane strength winds lie within a range of 300 to 600. Within the error of the data, the value for Re_r could reach as high as 1300.

In the intermediate roughness regime, the concavity of the scaling models from Garratt (1992) and Zilitinkevich et al. (2001) appears to be the opposite direction to the temperature data, although the great uncertainty in these measurements makes this observation more speculative than definitive. For the water vapor data, however, the upward concavity seems qualitatively correct in the intermediate regime, but the relative magnitudes are somewhat problematic. Again, the uncertainty in the measurements prevents any definitive observation about the curvature.

The smoother flows correspond to lower wind speeds and less developed wave fields. In the smoother flows, Zilitinkevich et al. (2001) predict larger temperature roughness lengths and, arguably, larger water vapor roughness lengths (lower ratios), which correspond to larger heat and mass fluxes than the data suggest. In rougher flows, their model predicts increasingly smaller scalar roughness lengths and consequently smaller fluxes. At low wind speeds, the interfacial fluxes are expected to dominate the total surface fluxes. At higher wind speeds, the interfacial flux may be less important because the sea spray-mediated fluxes may be significant (e.g., Andreas et al. 2008). Our model, which does not account for spray-mediated fluxes, produces ratios slightly higher than the data suggest. This means that our estimated fluxes do not account for more than the total measured fluxes for a given flow roughness. Although physically intuitive, there may be an issue with spurious correlation in these plots (e.g., Hicks 1978; Kenney 1982), as both nondimensional groups share the common variable z_m. Despite this concern, our model appears to agree with the available data as well as, if not better than, these previous models.

4. Results

In this section, the dependence of the scalar roughness lengths on the wave field is considered. Before discussing the wave-age dependence, however, we first present the roughness lengths for a constant fetch of 100 km. These roughness lengths for momentum, temperature, and water vapor are presented in Fig. 4a. At the lowest wind speeds and corresponding friction velocities, the roughness lengths approach the values for the smooth limit, which is also shown for z_m. The flow departs from the smooth limit for almost all but the lowest wind speeds. Between friction velocities of 0.2 and 0.5 m s^{-1}, the effective Charnock coefficient is below the classical value 0.011 (Charnock 1955), which is also shown for reference. For $0.6 < u_* < 1.5$ m s^{-1}, the effective Charnock coefficient is greater than 0.011. Eventually, the roughness length for momentum begins to plateau, resulting in a decreasing effective Charnock coefficient.

The roughness lengths for temperature and water vapor follow a simpler relationship with friction velocity. They follow the smooth flow limit closely until about 0.25 m s^{-1}. Between 0.25 and 0.7 m s^{-1}, the roughness lengths transition to a new relationship, which remains almost undisturbed after 0.7 m s^{-1}. This departure is much less pronounced than the momentum case because these scalar roughness lengths are monotonically decreasing in all three regimes: smooth, transition, and fully rough. These regimes can further be seen in Fig. 4b (around $U_{10} = 7$ m s^{-1} and $U_{10} = 25$ m s^{-1}), which shows the nondimensional roughness lengths of temperature and water vapor in wall coordinates. For the cases $\Delta\theta = 0$°C and $\Delta\theta = -3$°C, the roughness lengths approach their smooth flow limits at the lowest wind speeds. From 7 to about 25 m s^{-1}, nondimensional roughness lengths increase, and after 25 m s^{-1}, they are nearly constant. In the stably stratified case, $\Delta\theta = 3$°C, the nondimensional roughness at low wind speeds departs substantially from the neutral, smooth flow limit. This departure is partly due to the different Prandtl and Schmidt numbers with a colder surface temperature but is mostly due to the stability functions. As seen in Fig. 1a, the drag coefficient drops off rapidly at low wind speeds for the stably stratified cases. The vertical axis in Fig. 4b is scaled with the friction velocity. Therefore, as the surface stress drops off rapidly, the nondimensional roughness lengths also fall below their neutral, smooth limit values. At the highest wind speeds, stratification has less influence on the roughness lengths, so the spread is mostly due to the temperature dependence of the Prandtl and Schmidt numbers.

The influence of the wave field on the scalar roughness lengths will now be reported in terms of the inverse wave age, $\Omega = U_{10}/c_p$, where c_p is the phase speed of the peak wave. Figures 5a and 5b show the nondimensional roughness lengths for temperature and water vapor, respectively. For all wind speeds, the fully developed sea

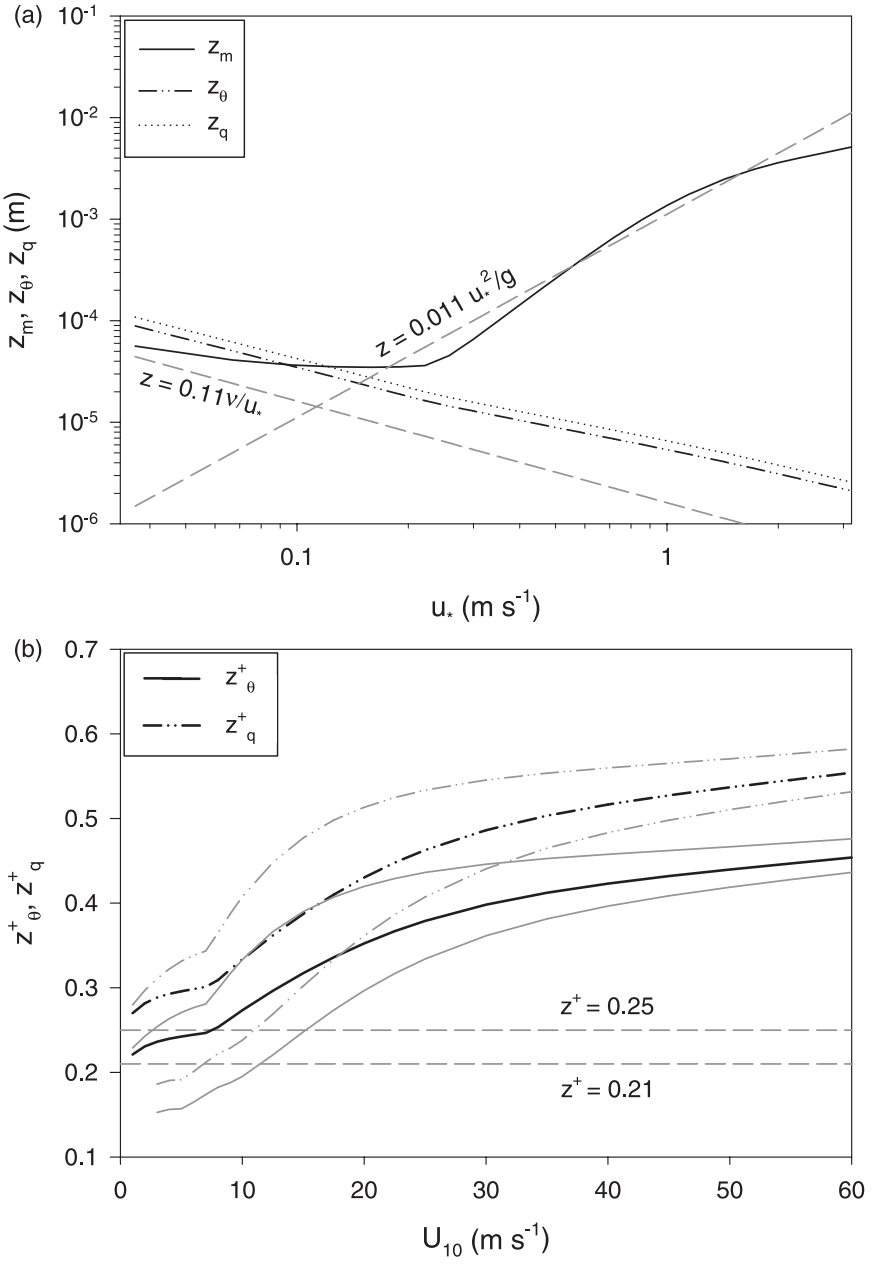

FIG. 4. (a) Roughness lengths for momentum (solid) and temperature (dashed–dotted) and water vapor (dotted) as a function of the friction velocity for $\Delta\theta = 0$°C, plotted with the smooth flow limit (downward, gray dashed) and Charnock relation (upward, gray dashed). (b) Nondimensional roughness lengths for temperature (solid) and water vapor (dashed–dotted) in wall coordinates as a function of wind speed for $\Delta\theta = 0$°C (black), −3°C (upper gray) and 3 (lower gray).

state ($\Omega = 0.84$) produces the greatest nondimensional scalar roughness, whereas the youngest sea state ($\Omega = 15$) produces the smallest nondimensional scalar roughness. For wind–wave equilibrium, an implicit assumption in the stress model used here, the sea state appears to have less of an effect than stratification and surface temperature (see Fig. 4b). At low to moderate wind speeds, the sea state does still appear to contribute to the scalar roughness length variability. Interestingly, this spread narrows at the higher wind speeds, corresponding to the saturation of the drag of the coefficient. Therefore, any reduction in the drag may be accompanied by a compensating limit on the interfacial heat and moisture fluxes. This behavior is also depicted in Fig. 1d.

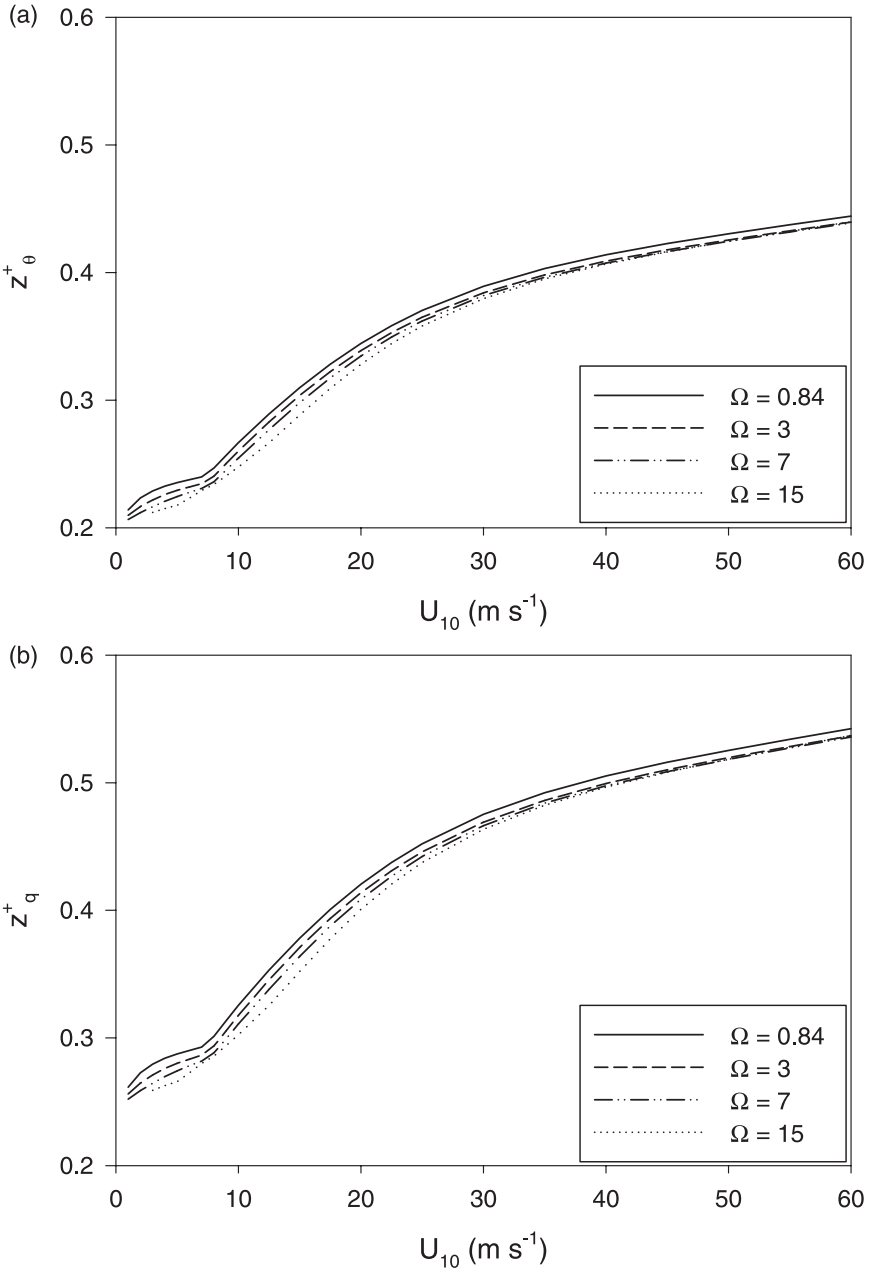

FIG. 5. (a) Nondimensional roughness lengths of temperature and (b) water vapor in wall coordinates as a function of wind speed for $\Delta\theta = 0$ and inverse wave age, $\Omega = U_{10}/c_p$ for $\Omega =$ 0.84 (solid), 3 (dashed), 7 (dashed–dotted), and 15 (dotted).

Finally, the flux scale approximations employed above imply surface flux components that are not due to molecular forces. Figures 6a and 6b respectively show the fractions of the molecular and nonmolecular surface fluxes for a 10-m fetch and a 100-km fetch. The relative fractions are the same for both the sensible heat and the water mass fluxes. In fact, the fraction of the total scalar flux due to molecular forces is identical for all scalars when using this formulation. At both fetches, the molecular flux component only accounts for about half of the total scalar flux by a wind speed of 25 m s^{-1}. At 50 m s^{-1}, the nonmolecular forces account for roughly three-fourths of the scalar flux.

While the nonmolecular contributions may seem to be a rather large fraction, they are actually substantially lower than the nonmolecular fractions of the momentum

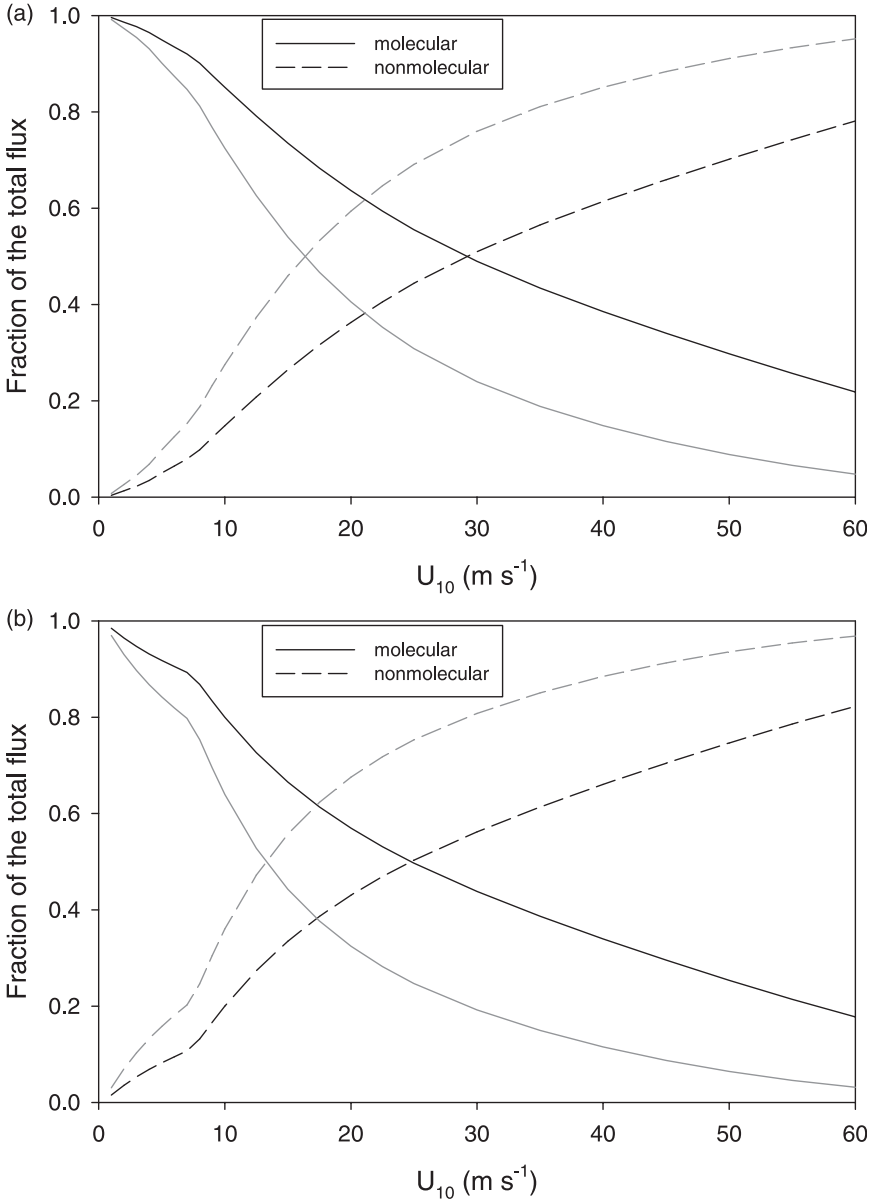

FIG. 6. The fraction of the molecular (solid) and nonmolecular (dashed) components of the surface fluxes for both sensible heat and water mass (black) and momentum (gray) at (a) 10-m and (b) 100-km fetch.

flux (also shown in Fig. 6 for reference). Under this formulation, the scalar flux fractions would be equal to the momentum flux fractions only if the total scalar fluxes were equal to the square root of the individual flux components squared: that is, $H = (H_{\text{mol}}^2 + H_w^2 + H_s^2)^{1/2}$ and $M = (M_{\text{mol}}^2 + M_w^2 + M_s^2)^{1/2}$. Compare this form to the one in Eq. (8), in which the scalar flux components are simply added linearly. In the absence of definitive evidence, Eq. (8) seems to be more intuitive, not only because of its form but also because of the corresponding relative fractions. There is no reason to believe that molecular forces should be equally important for both momentum and scalar fluxes. Scalar fluxes having a greater dependence on the molecular components compared to their momentum counterpart also makes sense. Nevertheless, even a finite nonmolecular component of the surface scalar fluxes remains controversial.

5. Conclusions

With the temperature and water vapor scales (θ_* and q_*) in addition to the total and viscous friction velocities

(u_* and u_{*_v}), the air–sea heat and water vapor fluxes at the surface can be modeled reasonably well. Even though the temperature and water vapor scales are approximated to be their smooth flow values, this first-order approximation appears to reproduce fluxes that are consistent with available experimental data. More importantly, this new framework incorporates nonmolecular components of the scalar fluxes without requiring an explicit theory or model. Certainly, this approach to modeling the air–sea fluxes encourages further refinement in the estimation of the temperature and water vapor scales in rough flows as well as explicit expressions for the potential interfacial components of the scalar fluxes. Because this approach explains the empirical data as well as, if not better than, the theoretical models of heat transfer over rigid, rough surfaces, there seems to be a compelling conclusion to draw: that the air–sea interfacial scalar fluxes at higher wind speeds may indeed deviate substantially from those predicted by previous theories of heat and mass transfer in rough flows.

Acknowledgments. We thank Ed Andreas for many helpful discussions and his diligent review of an early draft. This work was supported by ONR Grant N00014-05-1-0609 to FV.

REFERENCES

Andreas, E. L., and K. A. Emanuel, 2001: Effects of sea spray on tropical cyclone intensity. *J. Atmos. Sci.,* **58,** 3741–3751.

——, P. O. G. Persson, and J. E. Hare, 2008: A bulk turbulent air–sea flux algorithm for high-wind, spray conditions. *J. Phys. Oceanogr.,* **38,** 1581–1596.

Belcher, S. E., and J. C. R. Hunt, 1998: Turbulent flow over hills and waves. *Annu. Rev. Fluid Mech.,* **30,** 507–538.

Beljaars, A. C. M., and A. A. M. Holtslag, 1991: Flux parameterization over land surfaces for atmospheric models. *J. Appl. Meteor.,* **30,** 327–341.

Brutsaert, W., 1982: *Evaporation into the Atmosphere: Theory, History, and Applications*. D. Reidel, 299 pp.

Businger, J. A., J. C. Wyngaard, Y. Izumi, and E. F. Bradley, 1971: Flux-profile relationships in an atmospheric surface layer. *J. Atmos. Sci.,* **28,** 181–189.

Charnock, H., 1955: Wind stress on a water surface. *Quart. J. Roy. Meteor. Soc.,* **81,** 639–640.

Clayson, C. A., C. W. Fairall, and J. A. Curry, 1996: Evaluation of turbulent fluxes at the ocean surface using surface renewal theory. *J. Geophys. Res.,* **101** (C12), 28 503–28 513.

DeCosmo, J., K. B. Katsaros, S. D. Smith, R. J. Anderson, W. A. Oost, K. Bumke, and H. Chadwick, 1996: Air–sea exchange of water vapor and sensible heat: The Humidity Exchange over the Sea (HEXOS) results. *J. Geophys. Res.,* **101** (C5), 12 001–12 016.

Donelan, M. A., B. K. Haus, N. Reul, W. J. Plant, M. Stiassnie, H. C. Graber, O. B. Brown, and E. S. Saltzman, 2004: On the limiting aerodynamic roughness of the ocean in very strong winds. *Geophys. Res. Lett.,* **31,** L18306, doi:10.1029/2004GL019460.

Drennan, W. M., J. A. Zhang, J. R. French, C. McCormick, and P. G. Black, 2007: Turbulent fluxes in the hurricane boundary layer. Part II: Latent heat flux. *J. Atmos. Sci.,* **64,** 1103–1115.

Elfouhaily, T., B. Chapron, K. Katsaros, and D. Vandemark, 1997: A unified directional spectrum for long and short wind-driven waves. *J. Geophys. Res.,* **102** (C7), 15 781–15 796.

Emanuel, K. A., 1995: Sensitivity of tropical cyclones to surface exchange coefficients and a revised steady-state model incorporating eye dynamics. *J. Atmos. Sci.,* **52,** 3969–3976.

Fairall, C. W., E. F. Bradley, J. S. Godfrey, G. A. Wick, J. B. Edson, and G. S. Young, 1996a: Cool-skin and warm-layer effects on sea surface temperature. *J. Geophys. Res.,* **101** (C1), 1295–1308.

——, A. A. Grachev, A. J. Bedard, and R. T. Nishiyama, 1996b: Wind, wave, stress, and surface roughness relationships from turbulence measurements made on R/P FLIP in the SCOPE experiment. NOAA Tech. Memo. ERL ETL-268, 37 pp.

——, A. B. White, J. B. Edson, and J. E. Hare, 1997: Integrated shipboard measurements of the marine boundary layer. *J. Atmos. Oceanic Technol.,* **14,** 338–359.

——, J. E. Hare, J. B. Edson, and W. McGillis, 2000: Parameterization and micrometeorological measurement of the air–sea gas transfer. *Bound.-Layer Meteor.,* **96,** 63–106.

——, E. F. Bradley, J. E. Hare, A. A. Grachev, and J. B. Edson, 2003: Bulk parameterization of air–sea fluxes: Updates and verification for the COARE algorithm. *J. Climate,* **16,** 571–591.

Garratt, J. R., 1992: *The Atmospheric Boundary Layer*. Cambridge University Press, 316 pp.

Grachev, A., C. W. Fairall, and E. F. Bradley, 2000: Convective profile constants revisited. *Bound.-Layer Meteor.,* **94,** 495–515.

Hicks, B., 1978: Some limitations of dimensional analysis and power laws. *Bound.-Layer Meteor.,* **14,** 567–569.

Hinze, J. O., 1975: *Turbulence*. 2nd ed. McGraw-Hill, 790 pp.

Kenney, B. C., 1982: Beware of spurious self-correlations! *Water Resour. Res.,* **18,** 1041–1048.

Kudryavtsev, V. N., and V. K. Makin, 2007: Aerodynamic roughness of the sea surface at high winds. *Bound.-Layer Meteor.,* **125,** 289–303, doi:10.1007/s10546-007-9184-7.

Large, W. G., and S. Pond, 1982: Sensible and latent heat flux measurements over the ocean. *J. Phys. Oceanogr.,* **12,** 464–482.

Liu, W. T., K. B. Katsaros, and J. A. Businger, 1979: Bulk parameterization of air–sea exchanges of heat and water vapor including the molecular constraints at the interface. *J. Atmos. Sci.,* **36,** 1722–1735.

Makin, V. K., and C. Mastenbroek, 1996: Impact of waves on air–sea exchange of sensible heat and momentum. *Bound.-Layer Meteor.,* **79,** 279–300.

——, V. N. Kudryavtsev, and C. Mastenbroek, 1995: Drag of the sea-surface. *Bound.-Layer Meteor.,* **73,** 159–182.

Mueller, J. A., and F. Veron, 2009: Nonlinear formulation of the bulk surface stress over breaking waves: Feedback mechanisms from air-flow separation. *Bound.-Layer Meteor.,* **130,** 117–134, doi:10.1007/s10546-008-9334-6.

Owen, P. R., and W. R. Thomson, 1963: Heat transfer across rough surfaces. *J. Fluid Mech.,* **15,** 321–334.

Perrie, W., E. L. Andreas, W. Q. Zhang, W. B. Li, J. Gyakum, and R. McTaggart-Cowan, 2005: Sea spray impacts on intensifying midlatitude cyclones. *J. Atmos. Sci.,* **62,** 1867–1883.

Powell, M. D., P. J. Vickery, and T. A. Reinhold, 2003: Reduced drag coefficient for high wind speeds in tropical cyclones. *Nature,* **422,** 279–283, doi:10.1038/nature01481.

Sahlee, E., A.-S. Smedman, U. Högström, and A. Rutgersson, 2008: Reevaluation of the bulk exchange coefficient for humidity at sea during unstable and neutral conditions. *J. Phys. Oceanogr.,* **38,** 257–272.

Smith, R. K., M. T. Montgomery, and S. Vogl, 2008: A critique of Emanuel's hurricane model and potential intensity theory. *Quart. J. Roy. Meteor. Soc.,* **134,** 551–561, doi:10.1002/qj.241.

Soloviev, A. V., and P. Schluessel, 1994: Parameterization of the cool skin of the ocean and of the air–ocean gas transfer on the basis of modeling surface renewal. *J. Phys. Oceanogr.,* **24,** 1339–1346.

Sullivan, P. P., and J. C. McWilliams, 2002: Turbulent flow over water waves in the presence of stratification. *Phys. Fluids,* **14,** 1182–1195, doi:10.1063/1.1447915.

Taylor, P. K., and M. J. Yelland, 2000: On the apparent ''imbalance'' term in the turbulent kinetic energy budget. *J. Atmos. Oceanic Technol.,* **17,** 82–89.

van Driest, E. R., 1956: On turbulent flow near a wall. *J. Aeronaut. Sci.,* **23,** 1007–1011.

Veron, F., W. K. Melville, and L. Lenain, 2008: Wave-coherent air–sea heat flux. *J. Phys. Oceanogr.,* **38,** 788–802.

Zhang, J. A., P. G. Black, J. R. French, and W. M. Drennan, 2008: First direct measurements of enthalpy flux in the hurricane boundary layer: The CBLAST results. *Geophys. Res. Lett.,* **35,** L14813, doi:10.1029/2008GL034374.

Zilitinkevich, S. S., A. A. Grachev, and C. W. Fairall, 2001: Scaling reasoning and field data on the sea surface roughness lengths for scalars. *J. Atmos. Sci.,* **58,** 320–325.